# Implications of Charge Penetration for the Heteroatom-Containing Organic Semiconductors
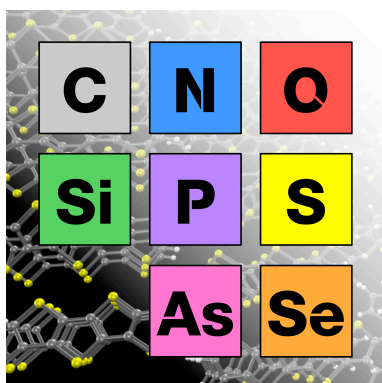
Ganna Gryn'ova and Clémence Corminboeuf*

*Institut des Sciences et Ingénierie Chimiques, École polytechnique fédérale de Lausanne, CH-1015 Lausanne, Switzerland*

**Abstract**

The non-covalent interactions of neutral π-conjugated cores, pertinent to organic semiconductor materials, are intimately related to their charge transport properties and involve a subtle interplay of dispersion, Pauli repulsion and electrostatic contributions. Realising structural arrangements that are both energetically preferred and sufficiently conductive is a challenge. We tackle this problem by means of charge penetration contribution to the interaction energy, boosted in systems containing large heteroatoms (e.g., sulphur, selenium, phosphorus, silicon and arsenic). We find that in both the model and 'realistic' dimers of such heteroatom-containing cores dispersion is balanced out by the exchange and interaction energy is instead governed by substantial charge penetration. These systems also feature stronger electronic couplings compared to the dispersion-driven dimers of oligoacenes and/or the herringbone assemblies. Thus, charge penetration, enhanced in the π-conjugated cores comprising larger heteroatoms, arises as an attractive strategy towards potentially more stable and efficient organic electronic materials.

**TOC**

Many monomers of interest for organic semiconductor applications are π-conjugated neutral compounds, thus their intermolecular interactions[1-4] involve appreciable Pauli repulsion and attractive London dispersion.[5,6,7] Their charge transport properties depend on the strength of the electronic coupling between adjacent cores, which in turn has been shown to correlate with the exchange component of the total interaction energy.[6,8] While the highest coupling is expected for perfectly cofacial π-stacked monomers, this packing is hardly ever realised in practice precisely because the destabilising exchange in this configuration is also maximum.[6] Numerous strategies exist to impose the energetically less favoured but more transport-efficient packing through side chain engineering.[9] Regarding the bare cores, Pauli repulsion can be overcome by harnessing attractive dispersion in, for example, increasingly large oligoacenes,[10] which also involve substantial charge penetration.[5] The latter occurs when diffuse electron clouds of the interacting entities overlap (interpenetrate) and the nuclei of one molecule (or fragment) become less shielded by its own electron density. As such, they experience Coulombic attraction towards the electron density of the other interacting species. Due to quantum nature of the electron, this electron-nuclei attraction is stronger than the electron-electron and nuclei-nuclei repulsions. At relatively large interaction distances this effect is virtually non-existent and electrostatic interaction is due to attraction or repulsion between their permanent multipoles, quantified by the multipolar expansion, *i.e.* the classical Stone's distributed multipole analysis (DMA).[11] However, at a sufficiently short range the classical multipole picture breaks down since electrostatics becomes dominated by stabilising charge penetration, independent on the polarity of interacting multipoles.

Charge penetration might seem subtle at first, yet, as illustrated by Sherrill and co-workers,[12] it is responsible for surprising electrostatic stabilisation of the substituted benzene dimers independent on the electronic nature of substituents. The crucial role of charge penetration has been demonstrated in the energetics of the benzene•••$H_2$ complexes,[13] dimers of polycyclic aromatic hydrocarbons[14] and nucleobase pairs[15,16] and isomerisation of paracyclophanes,[17] and prompts the development of new schemes incorporating it into the modern classical force fields.[18] This raises a question of whether the charge penetration is or can be made sufficiently large to dominate the non-covalent interactions of organic semiconductors and ultimately promote the assemblies with improved charge transport characteristics.

Both the charge penetration and the exchange depend on the extent of overlap between the total electron densities (all occupied orbitals) of the interacting species,[6,19] while the electronic coupling is generally approximated from the relevant frontier orbitals, e.g. the highest occupied molecular orbitals (HOMOs) for hole transport.[20-22] Dependence of charge penetration on the overlap between

electron densities suggests it should also be sensitive to the nature of atomic species, constituting the molecule. In this regard, many $\pi$-conjugated cores, found in organic semiconductor crystals, contain sulphur, nitrogen and other heteroatoms.[23-25] The impact of heteroatom identity on the geometric and electronic structure of these cores is well appreciated.[26] Beyond the monomer, heteroatoms affect the intermolecular interaction energies, molecular packing and charge mobility.[27-33] For instance, the interaction energies in the dimers of nitrogen-containing heterocycles are different from the all-carbon analogues and depend on the position of the heteroatom(s). This is attributed to the contracted electronic density of nitrogen compared to carbon and results in reduced (in magnitude) exchange and weaker electronic coupling.[6,34,35]

In the present work we explore how the stability of systems, relevant to the field of organic semiconductors, can be promoted by means of charge penetration and without sacrificing their charge transport characteristics. In this respect, we investigate a range of $\pi$-conjugated cores containing carbon, silicon, pnictogens and chalcogens from the 2-4 periods of the periodic table (Chart 1A). Syntheses, structures and charge transport properties for many of these or similar systems have been reported in the literature.[23,32,36-40] Geometries of isolated monomer cores were optimised at the PBE0/def2-SVP level and their dimers were constructed from optimised monomers by translating one cofacial coplanar monomer with respect to another along the perpendicular and longitudinal axes, as shown in Chart 1B. For several cores, representative 'realistic' dimers were taken from reported crystal structures (see Ref. 5 in the Supporting Information). For each dimer geometry, the total interaction energy was evaluated using the method, considered a bronze standard for non-covalent interactions,[41] – the zeroth-order symmetry-adapted perturbation theory (SAPT0) with jun-cc-pVDZ basis,[42] which allows decomposing the total interaction energy $E_{tot}$ into the exchange $E_{exch}$, electrostatic $E_{elst}$, dispersion $E_{disp}$ and induction $E_{ind}$ components. The distributed multipole analyses (DMA)[11] computations were performed at the HF/6-311G** level. Charge penetration $E_{CPen}$ was evaluated as the difference between $E_{elst}$ and the DMA electrostatic term $E_{DMA}$. Finally, the electronic couplings were computed at the PBE0-dDsC[43]/DZP level of theory using ADF2014.[44-46] For clarity, throughout the manuscript we only discuss the electronic couplings for hole transfer, $V_{+}$; however, for pnictogen-containing materials the $n$-type transport is also relevant, thus we have verified the established trends for the electronic couplings for electron transfer, $V_{-}$, in their dimers (see Figure S5C and D in the Supporting Information). In all computations, appropriate corrections were employed to account for relativistic effects in Se and As. A detailed description of these procedures is given in the Supporting Information.
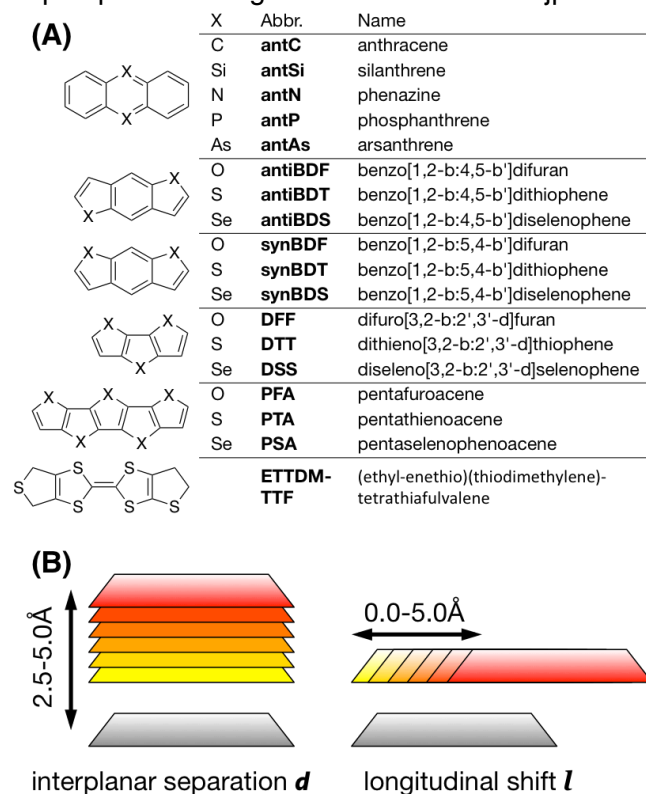
| X | Abbr. | Name |
|---|---|---|
| C | **antC** | anthracene |
| Si | **antSi** | silanthrene |
| N | **antN** | phenazine |
| P | **antP** | phosphanthrene |
| As | **antAs** | arsanthrene |
| O | **antiBDF** | benzo[1,2-b:4,5-b']difuran |
| S | **antiBDT** | benzo[1,2-b:4,5-b']dithiophene |
| Se | **antiBDS** | benzo[1,2-b:4,5-b']diselenophene |
| O | **synBDF** | benzo[1,2-b:5,4-b']difuran |
| S | **synBDT** | benzo[1,2-b:5,4-b']dithiophene |
| Se | **synBDS** | benzo[1,2-b:5,4-b']diselenophene |
| O | **DFF** | difuro[3,2-b:2',3'-d]furan |
| S | **DTT** | dithieno[3,2-b:2',3'-d]thiophene |
| Se | **DSS** | diseleno[3,2-b:2',3'-d]selenophene |
| O | **PFA** | pentafuroacene |
| S | **PTA** | pentathienoacene |
| Se | **PSA** | pentaselenophenoacene |
| | **ETTDM-TTF** | (ethyl-enethio)(thiodimethylene)-tetrathiafulvalene |

**Chart 1. (A)** Investigated π-conjugated cores containing heteroatoms, as well as their common chemical names and abbreviations, used throughout this work. (B) Schematic representation of the dimer construction: interplanar separation $d$ and longitudinal shift $l$ varied with a 0.25Å step size.

**What are the relationships between the exchange, charge penetration and the electronic coupling?** Figure 1 shows how the electronic coupling (A) and interaction energy terms (B) change with the longitudinal shift (at fixed interplanar distance of 3.50Å) in two representative systems, anthracene (antC) and pentathienoacene (PTA). The electronic coupling, $V_+$, of both systems displays an oscillating behaviour with distinct extrema, corresponding to dimer geometries that lead to the most and the least effective frontier orbital overlaps between the monomers. In antC and PTA dimers (shown here, and other studied systems, for which the results are given in the Supporting Information), the induction component of the interaction energy is rather small (approx. 3% of the total energy in absolute terms); dispersion is the main stabilising interaction (~45-50%), decaying monotonously with increasing long-axis shift. The exchange is the main repulsive interaction (~33-38%) and in both systems it decays with increasing shift in oscillatory fashion that is much more pronounced in PTA. Charge penetration is stabilising and is larger in absolute terms (*ca.* 15-18%) than the classical electrostatics (DMA, ~0-6%) in both antC and PTA, and, similarly to the exchange term, its oscillating behaviour is significantly amplified in PTA compared to antC. This is due to the fact that both energetic terms arise from the interactions between the total electron

5

densities of two monomers. The electron density is rather uniform in anthracene, but has a distinct structure in PTA (Figure 1A). Furthermore, *x*-axis positions (values of the longitudinal shift) of the minima and maxima of $V_+$ do not match those of the exchange and charge penetration (and ultimately the total interaction energy) exactly. The reason is precisely the fact that the electronic coupling depends on the overlap of only the frontier orbitals, while the aforementioned interactions are due to the overlap of all occupied orbitals of the monomers. We also note that the exchange and charge penetration increase with increasing system size and in particular the increasing number of heavier heteroatoms in it (Figure 1C). Behaviour of the electronic coupling is more complex since it depends on the symmetry and spatial localisation of the frontier orbitals, distinctly different in the four considered cores (see Figure S2 and discussion in the Supporting Information), rather than the sum of all occupied orbitals.
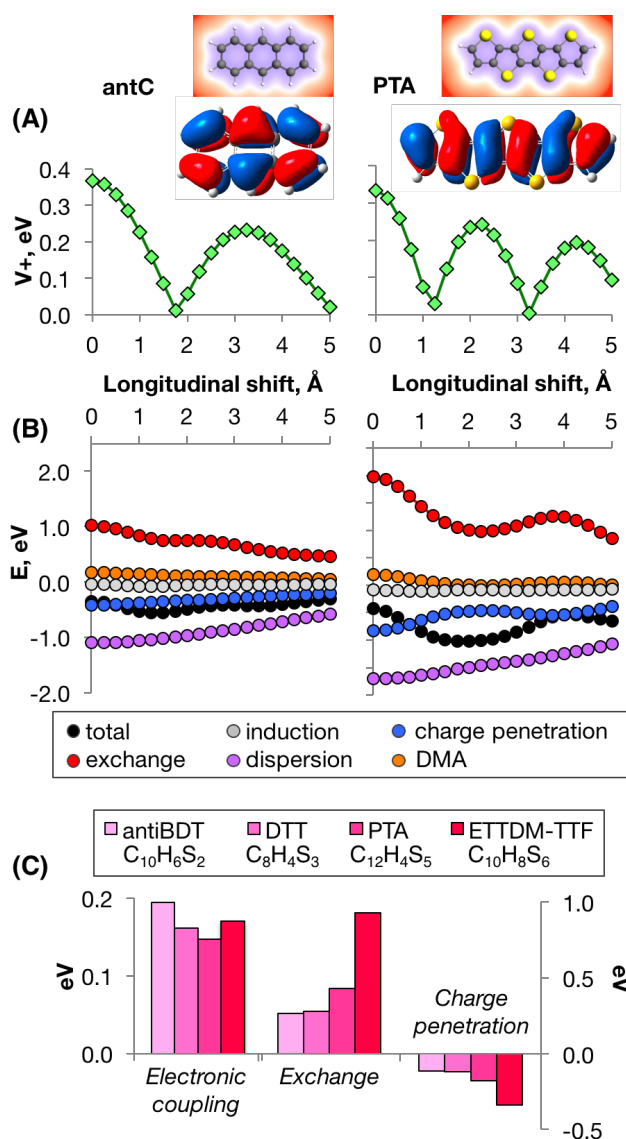
**Figure 1.** Computed electronic couplings (A), total interaction energies and their components (B) for antC (left) and PTA (right) dimers with fixed intermonomer distance $d = 3.50$Å and varying longitudinal shift $l$ ($x$-axis). Also shown are plots of the monomer's highest occupied molecular orbital (HOMO, isovalue = 0.02) and the total electron density, projected onto a cut plane at 1Å distance from molecular plane ($10^{-5}$ to 1.0 range, logarithmic scale). (C) Computed electronic couplings, exchange and charge penetration contributions to the total interaction energies for identical dimers ($d = 4.00$Å, $l = 1.00$Å for ETTDM-TTF and 0.00Å for other dimers) of four sulphur-containing monomers. Electronic couplings are computed at the PBE0-dDsC/DZP level, interaction energies – at SAPT0/jun-cc-pVDZ level and DMA – at the HF/6-311G** level, orbital and density plots – at the PBE0/def2-SVP of theory.

**How does the type of heteroatom influence the charge penetration?** Results in Figure 2A demonstrate that for the perfectly cofacial geometrically identical dimers ($d = 3.50$Å and $l = 0.00$Å) of several tricyclic $\pi$-conjugated heteroaromatic cores their ordering in terms of the magnitude of $V_+$, $E_{exch}$ and $E_{CPen}$ follows several trends. These trends arise from the properties of the heteroatoms, included in these otherwise fairly similar cores. We find that the electronic coupling, exchange and charge penetration increase down the group in the periodic table: from carbon to silicon in group 14, N<P<As for pnictogens and O<S<Se for chalcogens. These relationships persist for increasing interplanar separation (Figure S3A in the Supporting Information) and are recognisably the trends of increasing atomic[47] and van der Waals (vdW)[48] radii of these elements.
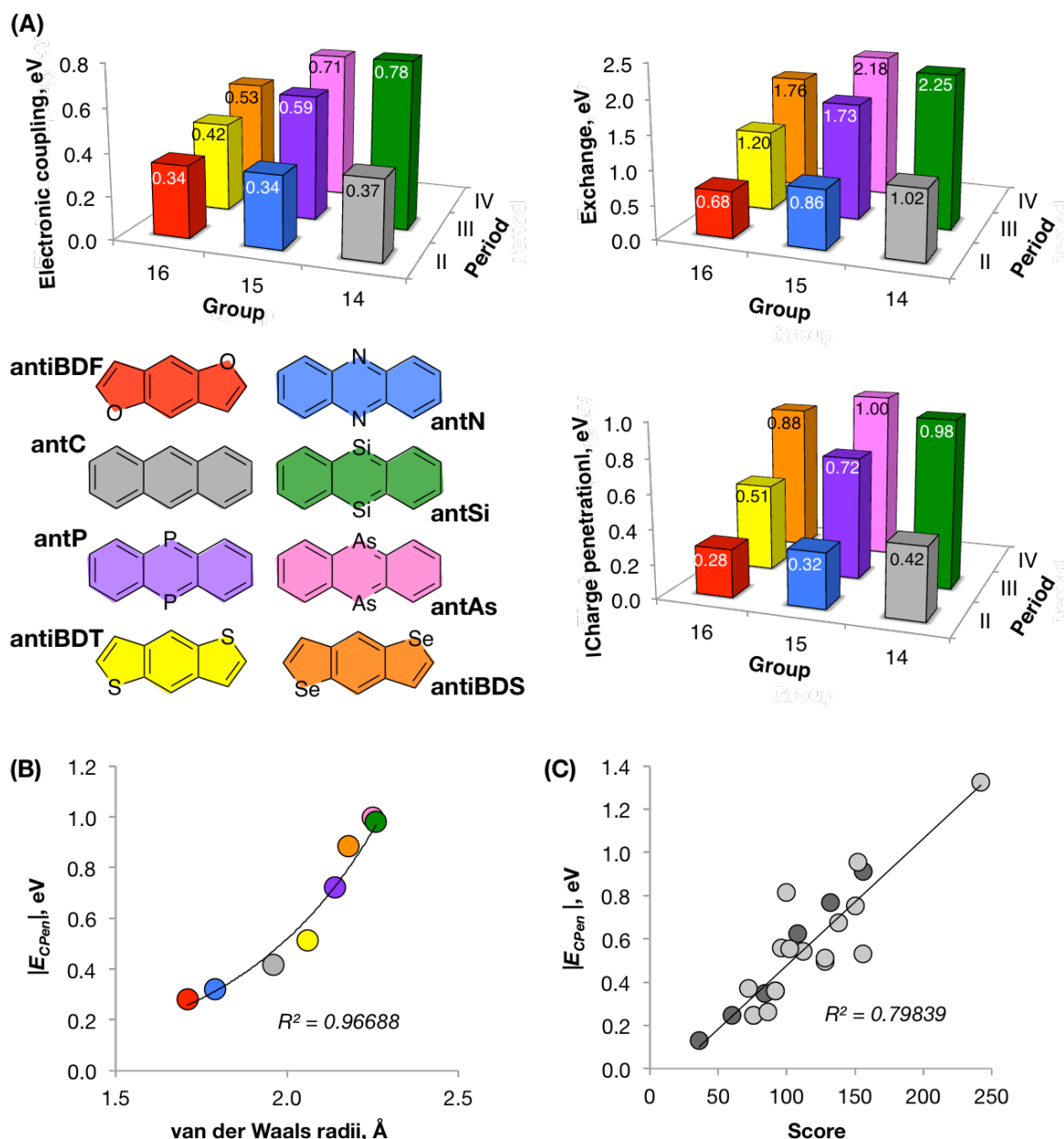
**Figure 2.** (A) Computed electronic couplings, exchange and charge penetration contributions to the total interaction energies for the dimers of eight tricyclic cores in identical geometries ($d$ = 3.50Å and $l$ = 0.00Å) for each core depending on the location of the corresponding heteroatom in the periodic table (group and period). (B) Correlations between computed charge penetration contributions in identical dimers and atomic van der Waals radii[48] (trendline of an exponential fit). (C) Correlations between computed charge penetration contributions in the local minima dimers of all studied cores (acenes are shown in dark grey, heteroatomic cores – in light grey) and their monomer scores (trendline of a linear fit). Electronic couplings are computed at the PBE0-dDsC/DZP level, interaction energies – at SAPT0 level with aug-cc-pVDZ (antAs and antiBDS) and jun-cc-pVDZ (other cores) basis sets, DMA – at the HF/6-311G** (ECP28MDF for heavy atoms) level of theory.

8

Overall, we find significant correlations between the amount of charge penetration in these similarly sized cores and the radii of their corresponding heteroatoms (Figure 2B, see also Table S2 and Figure S3B in the Supporting Information). However, our analysis so far has been limited to cores that essentially differ only in two heteroatoms, and dimers having identical geometries. In order to encompass cores of more dissimilar sizes and atomic compositions, a simple score function can be employed:

$$Score = \sum_i n_i Z_i \qquad \text{Eq. 1}$$

where $n_i$ is the quantity of non-hydrogen atoms $i$ (carbon, sulphur, nitrogen, etc.) in the molecule and $Z_i$ is the atomic number of atom $i$. Figure 2C illustrates the correlation between this parameter for all cores in Chart 1 and, additionally, several acenes (benzene to hexacene),[10] and the extent of charge penetration in their local minima dimers. The latter are defined as minima on the computed potential energy surfaces in the ranges of 2.50-5.00Å for intermonomer distance $d$ and 0.00-5.00Å for longitudinal shift $l$ (fixed zero transversal shift and pitch, yaw and roll angles, see also Table S3 in the Supporting Information). Obviously, systems, investigated in this work, are largely limited to flat π-conjugated cores (with the exception of ETTDM-TTF) and are assembled into co-parallel dimers, thus additional (most likely, geometric) factors would be necessary to predict the extent of charge penetration in more diverse systems. Nonetheless, our results unambiguously demonstrate that cores, containing larger atoms, benefit from greater overlap of electronic clouds at short interaction distances and, correspondingly, their dimers experience greater stabilisation from charge penetration.

**What is the contribution of charge penetration to the total interaction energy?** In absolute terms, charge penetration is smaller (15-20%) than the exchange and dispersion (approx. 35-45% each, see representative examples in Figure 1, as well as Figure S4 in the Supporting Information). In order to elucidate the role that charge penetration plays in the interactions between the π-conjugated heteroaromatic cores, we have examined the interaction energies for the local minima dimers of representative heteroatom-containing monomers (Chart 1). We have also included the oligoacene cores, recently studied using a very similar computational approach by Brédas *et al.*[10] Using the contributions from SAPT0 energy decomposition, we represent the total interaction energy as:

$$E_{tot} = E_{elst} + E_{non-elst} = (E_{CPen} + E_{DMA}) + (E_{exch} + E_{disp} + E_{ind}) \qquad \text{Eq. 2}$$

Results in Figure 3 reveal several trends in the behaviour of total interaction energies, their components and the electronic couplings in the local minima dimers of various cores, which on this basis can be organised as follows:

(A) oligoacene cores;

(B) anthracene-like cores containing C, Si and pnictogens;

(C) chalcogen-containing benzodiheterophene and pentaheteroacene cores.
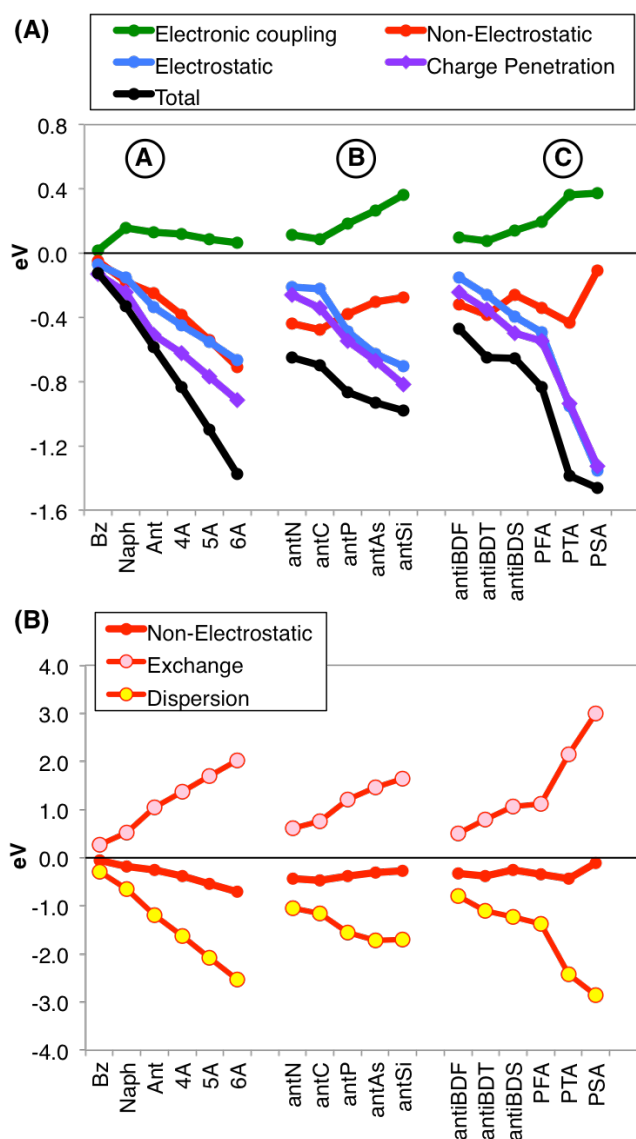


**Figure 3.** Computed interaction energy terms (as defined in Eq. 2) and the electronic couplings (A), as well as the non-electrostatic energy contributions (sans induction, B) for the local minima dimers of heteroatomic cores (see abbreviations in Chart 1A) in this work and oligoacenes from Ref. 10 (Bz – benzene, Ant – anthracene, Naph – naphthalene, 4A – tetracene, 5A – pentacene, 6A – hexacene, SAPT0/jun-cc-pVDZ method, see Table S3 in the Supporting Information for details). Electronic couplings are computed at the

10

PBE0-dDsC/DZP level, interaction energies – at SAPT0/aug-cc-pVDZ level and DMA – at the HF/6-311G** (ECP28MDF for heavy atoms) level of theory.

In all classes, charge penetration is the main stabilising contribution to $E_{elst}$. In systems, composed of more compact atoms (oligoacenes, antN, antiBDF), electrostatic contribution is smaller or roughly equal to the non-electrostatic contribution, which is driven by dispersion. Such systems lack appreciable direct overlap of their electronic clouds and thus comprise only moderate $E_{exch}$, $E_{CPen}$ and $V_+$. Notably, the electronic coupling in oligoacenes gradually declines with an increasing size of the conjugated system (from naphthalene to higher acenes) due to decreasing energy difference between the HOMO-1 and HOMO and increasing in-plane delocalisation of the frontier electronic density.[49] As we move to cores containing larger heteroatoms in increasing quantities (antP, antAs and antSi in class B, antiBDT, antiBDS and pentaheteroacenes in class C), the exchange interaction in their dimers intensifies and balances the dispersion out. As a result, their $E_{tot}$ is essentially governed by $E_{CPen}$. Furthermore, large $E_{CPen}$ and $E_{exch}$ in these systems are symptomatic of strong electronic coupling, which, however, can be impeded by unfavourable long-axis shifts between the monomers in a dimer (e.g., low $V_+$ in antiBDT compared to antiBDF in class C, for details see Table S3 and Figure S5A and B of the Supporting Information).

**Is charge penetration relevant to realistic systems?** Since our primary aim is to investigate how including heteroatoms in π-conjugated monomers affects the extent of charge penetration between them, we have employed a simple co-parallel cofacial dimer model and only varied two structural parameters ($d$ and $l$ in Chart 1B). However, in practice organic semiconductor crystals are rarely, if ever, composed of such 'well-behaved' dimer units. Instead, they feature a variety of architectures (brickwork, herringbone, discotic, etc.),[23] involve complex many-body interactions[50-52] that are not captured by SAPT0 analysis, and their charge transport properties are subject to energetic and structural disorder.[53] Nonetheless, to obtain at least a crude idea of how relevant charge penetration is to the behaviour of bulk material, we have investigated interactions in the dimers, extracted from experimental crystal structures, reported in the literature for several of the cores, considered in this work (Figure 4).
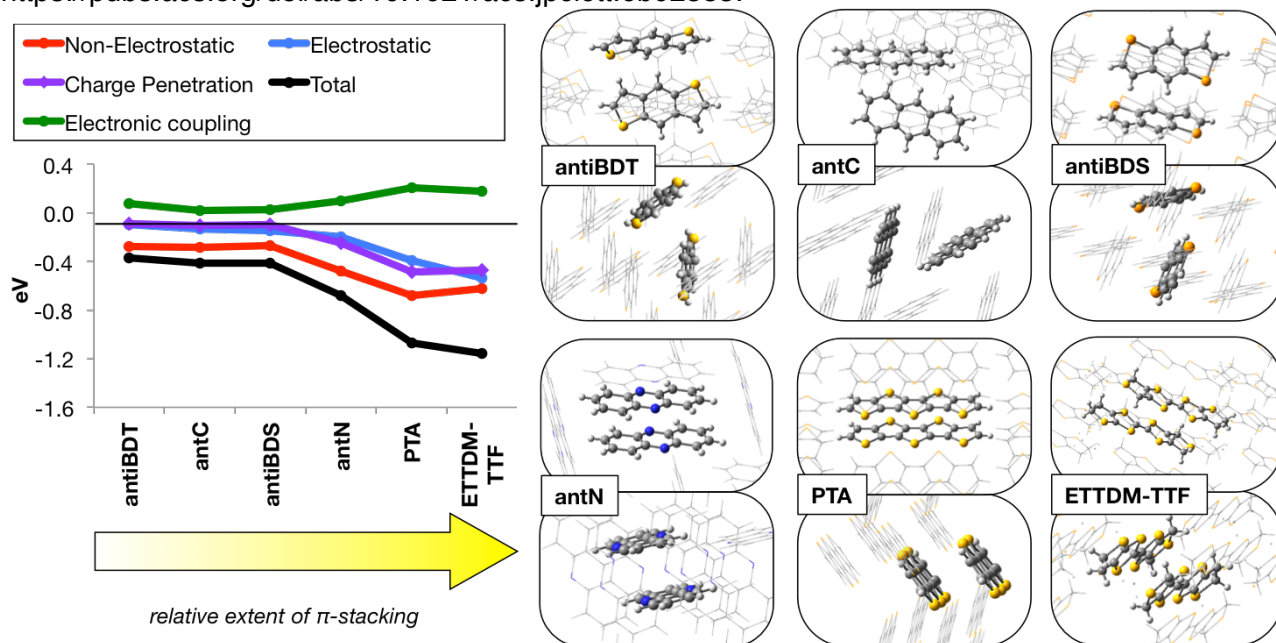
**Figure 4.** Computed interaction energies and their components (defined in Eq. 2), as well as the electronic couplings for the dimer configurations, taken from X-ray crystal structures (see Ref. 5 and Table S4 in the Supporting Information for details). For each monomer (see abbreviations in Chart 1A), experimental crystal structure (studied dimers are in ball-and-stick representation) is shown in two projections. Electronic couplings are computed at the PBE0-dDsC/DZP level, interaction energies – at SAPT0/aug-cc-pVDZ level and DMA – at the HF/6-311G** (ECP28MDF for heavy atoms) level of theory.

We find that when the cores are arranged in a herringbone manner (antiBDT, antC ant antiBDS), dispersion is the main driving force for stabilising their dimers, since in such geometries there is much less direct electron density overlap, *i.e.* less exchange and charge penetration, as well as lower electronic couplings. Within the antN crystal structure there exist co-parallel shifted dimers, however, the benefit from this arrangement for $E_{exch}$, $E_{CPen}$ and $V_+$ is moderate due to the contracted electronic density of nitrogen. Only in the sulphur-rich cores (PTA and ETTDM-TTF) with appreciable π-stacking in their crystals the exchange and charge penetration are large enough to compete with dispersion. As expected, the electronic coupling in such dimers is also substantial. Importantly, as noted above, our analysis does omit a number of important bulk effects. To establish the relevance of the computed trends in Figure 4, they should be compared to experimentally measures properties (e.g., charge mobilities), however, the lack of data, measured under similar conditions, precludes such comparison.

In summary, we show that charge penetration is the major stabilising component of electrostatic interactions in the dimers of π-conjugated monomers, containing various heteroatoms (N, P, As, O, S, Se, Si) and pertinent to organic electronics applications. Moreover, the larger the

12

heteroatoms, contained within a core, the greater (in absolute terms) are the charge penetration and the exchange contributions to the total interaction energy in its π-stacked dimer. Crucially, the exchange in these systems is considerable enough to balance the dispersion out and, at the same time, is indicative of potentially strong electronic coupling. In contrast, the non-covalent interactions in systems composed of compact C, O and N atoms (e.g., acenes and azaacenes)[6,10] and/or featuring the herringbone packing are driven by dispersion and afford only moderate electronic coupling, which decays with the increasing system size.[49] Thus, instead of increasing the size (e.g. adding extra aromatic rings) of the π-system to yield the dispersion-driven aggregates, more stable and potentially more efficient organic semiconductor materials can be built from the charge penetration dominated assemblies, comprising larger heteroatoms in their cores.

## ASSOCIATED CONTENT

### Supporting Information

Computational details, tables of data, used to produce the figures in this manuscript, additional figures, Cartesian coordinates for the optimised geometries, plots of highest occupied orbitals, 2D and 3D maps of computed interaction energies and electronic couplings for all investigated systems.

## AUTHOR INFORMATION

### Corresponding Author

*E-mail: clemence.corminboeuf@epfl.ch

### Notes

The authors declare no competing financial interest.

## ACKNOWLEDGEMENTS

## REFERENCES

[1] Grimme, S. Do Special Noncovalent π-π Stacking Interactions Really Exist? *Angew. Chem. Int. Ed.* **2008**, *47*, 3430-3434.

[2] Bloom, J. W. G.; Wheeler, S. E. Taking the Aromaticity out of Aromatic Interactions. *Angew. Chem. Int. Edi.* **2011**, *50*, 7847-7849.

[3] Fokin, A. A.; Gerbig, D.; Schreiner, P. R. σ/σ- and π/π-Interactions Are Equally Important: Multilayered Graphanes. *J. Am. Chem. Soc.* **2011**, *133*, 20036-20039.

[4] Martinez, C. R.; Iverson, B. L. Rethinking the Term ''pi-Stacking''. *Chem. Sci.* **2012**, *3*, 2191-2201.

[5] Sherrill, C. D. Energy Component Analysis of π Interactions. *Acc. Chem. Res.* **2012**, *46*, 1020-1028.

[6] Sutton, C.; Risko, C.; Brédas, J.-L. Noncovalent Intermolecular Interactions in Organic Electronic Materials: Implications for The Molecular Packing vs Electronic Properties of Acenes. *Chem. Mater.* **2015**, *28*, 3-16.

[7] Horn, P. R.; Mao, Y.; Head-Gordon, M. Defining the Contributions of Permanent Electrostatics, Pauli Repulsion, and Dispersion in Density Functional Theory Calculations of Intermolecular Interaction Energies. *J. Chem. Phys.* **2016**, *144*, 114107.

[8] Sutton, C.; Sears, J. S.; Coropceanu, V.; Brédas, J.-L. Understanding the Density Functional Dependence of DFT-Calculated Electronic Couplings in Organic Semiconductors. *J. Phys. Chem. Lett.* **2013**, *5*, 919-924.

[9] Mei, J.; Diao, Y.; Appleton, A. L.; Fang, L.; Bao, Z. Integrated Materials Design of Organic Semiconductors for Field-Effect Transistors. *J. Am. Chem. Soc.* **2013**, *135*, 6724-6746.

[10] Ryno, S. M.; Risko, C.; Brédas, J.-L. Noncovalent Interactions and Impact of Charge Penetration Effects in Linear Oligoacene Dimers and Single Crystals. *Chem. Mater.* **2016**, *28*, 3990-4000.

[11] Stone, A. J. Distributed Multipole Analysis, Or How to Describe a Molecular Charge Distribution. *Chem. Phys. Lett.* **1981**, *83*, 233-239.

[12] Hohenstein, E. G.; Duan, J.; Sherrill, C. D. Origin of the Surprising Enhancement of Electrostatic Energies by Electron-Donating Substituents in Substituted Sandwich Benzene Dimers. *J. Am. Chem. Soc.* **2011**, *133*, 13244-13247.

[13] Donchev, A. G. Ab Initio Study of the Effects of Orientation and Corrugation for $H_2$ Adsorbed on Polycyclic Aromatic Hydrocarbons. *J. Chem. Phys.* **2007**, *126*, 124706.

[14] Podeszwa, R.; Szalewicz, K. Physical Origins of Interactions in Dimers of Polycyclic Aromatic Hydrocarbons. *Phys. Chem. Chem. Phys.* **2008**, *10*, 2735-2746.

[15] Parker, T. M.; Hohenstein, E. G.; Parrish, R. M.; Hud, N. V.; Sherrill, C. D. Quantum-Mechanical Analysis of the Energetic Contributions to π-Stacking in Nucleic Acids versus Rise, Twist, and Slide. *J. Am. Chem. Soc.* **2013**, *135*, 1306-1316.

[16] Parker, T. M.; Sherrill, C. D. Assessment of Empirical Models versus High-Accuracy Ab Initio Methods for Nucleobase Stacking: Evaluating the Importance of Charge Penetration. *J. Chem. Theory Comput.* **2015**, *11*, 4197-4204.

[17] Xia, J. L.; Liu, S. H.; Cozzi, F.; Mancinelli, M.; Mazzanti, A. An Experimental Study on the Effect of Substituents on Aromatic–Aromatic Interactions in Dithia[3,3]-metaparacyclophanes. *Chem. Eur. J.* **2012**, *18*, 3611-3620.

[18] Wang, B.; Truhlar, D. G. Including Charge Penetration Effects in Molecular Modeling. *J. Chem. Theory Comput.* **2010**, *6*, 3330-3342.

[19] Freitag, M. A.; Gordon, M. S.; Jensen, J. H.; Stevens, W. J. Evaluation of Charge Penetration between Distributed Multipolar Expansions. *J. Chem. Phys.* **2000**, *112*, 7300-7306.

[20] Senthilkumar, K.; Grozema, F. C.; Fonseca Guerra, C.; Bickelhaupt, F. M.; Lewis, F. D.; Berlin, Y. A.; Ratner, M. A.; Siebbeles, L. D. A. Absolute Rates of Hole Transfer in DNA. *J. Am. Chem. Soc.* **2005**, *127*, 14894-14903.

[21] Troisi, A.; Orlandi, G. Dynamics of the Intermolecular Transfer Integral in Crystalline Organic Semiconductors. *J. Phys. Chem. A* **2006**, *110*, 4065-4070.

[22] Sánchez-Carrera, R. S.; Atahan, S.; Schrier, J.; Aspuru-Guzik, A. Theoretical Characterization of the Air-Stable, High-Mobility Dinaphtho[2,3-b:2′3′-f]thieno[3,2-b]-thiophene Organic Semiconductor. *J. Phys. Chem. C* **2010**, *114*, 2334-2340.

[23] Takimiya, K.; Nakano, M.; Sugino, H.; Osaka, I. Design and Elaboration of Organic Molecules for High Field-Effect-Mobility Semiconductors. *Synt. Met.* **2016**, *217*, 68-78.

[24] Anthony, J. E.; Facchetti, A.; Heeney, M.; Marder, S. R.; Zhan, X.; n-Type Organic Semiconductors in Organic Electronics. *Adv. Mater.* **2010**, *22*, 3876-3892.

[25] Bendikov, M.; Wudl, F.; Perepichka, D. F. Tetrathiafulvalenes, Oligoacenenes, and Their Buckminsterfullerene Derivatives: The Brick and Mortar of Organic Electronics. *Chem. Rev.* **2004**, *104*, 4891-4945.

[26] Bloom, J. W. G.; Wheeler, S. E. Benchmark Torsional Potentials of Building Blocks for Conjugated Materials: Bifuran, Bithiophene, and Biselenophene. *J. Chem. Theory Comput.* **2014**, *10*, 3647-3655.

[27] Hutchinson, G. R.; Ratner, M. A.; Marks, T. J. Intermolecular Charge Transfer between Heterocyclic Oligomers. Effects of Heteroatom and Molecular Packing on Hopping Transport in Organic Semiconductors. *J. Am. Chem. Soc.* **2005**, *127*, 16866-16881.

[28] Huber, R. G.; Margreiter, M. A.; Fuchs, J. E.; von Grafenstein, S.; Tautermann, C. S.; Liedl, K. R.; Fox, T. Heteroaromatic π-Stacking Energy Landscapes. *J. Chem. Inf. Model.* **2014**, *54*, 1371-1379.

[29] Yan, L.; Zhao, Y.; Yu, H.; Hu, Z.; He, Y.; Li, A.; Goto, O.; Yan, C.; Chen, T.; Chen, R.; Loo, Y.-L.; Perepichka, D. F.; Meng, H.; Huang, W. Influence of Heteroatoms on the Charge Mobility of Anthracene Derivatives. *J. Mater. Chem. C,* **2016**, *4*, 3517-3522.

[30] Thorley, K. J.; Risko, C. On the Impact of Isomer Structure and Packing Disorder in Thienoacene Organic Semiconductors. *J. Mater. Chem. C* **2016**, *4*, 4040-4048.

[31] Chang, Y.-C.; Chen, Y.-D.; Chen, C.-H.; Wen, Y.-S.; Lin, J. T.; Chen, H.-Y.; Kuo, M.-Y.; Chao, I. Crystal Engineering for π-π Stacking via Interaction between Electron-Rich and Electron-Deficient Heteroaromatics. *J. Org. Chem.* **2008**, *73*, 4608-4614.

[32] Takimiya, K.; Kunugi, Y.; Konda, Y.; Niihara, N.; Otsubo, T. 2,6-Diphenylbenzo[1,2-b:4,5-b']dichalcogenophenes: A New Class of High-Performance Semiconductors for Organic Field-Effect Transistors. *J. Am. Chem. Soc.* **2004**, *126*, 5084-5085.

[33] Nakano, M.; Mori, H.; Shinamura, S.; Takimiya, K. Naphtho[2,3-b:6,7-b']dichalcogenophenes: Syntheses, Characterizations, and Chalcogene Atom Effects on Organic Field-Effect Transistor and Organic Photovoltaic Devices. *Chem. Mater.* **2012**, *24*, 190-198.

[34] Hohenstein, E. G.; Sherrill, C. D. Effects of Heteroatoms on Aromatic π-π Interactions: Benzene-Pyridine and Pyridine Dimer. *J. Phys. Chem. A* **2009,** *113,* 878-886.

[35] Wheeler, S. E.; Bloom, J. W. G. Anion-π Interactions and Positive Electrostatic Potentials of N-Heterocycles Arise from the Positions of the Nuclei, not Changes in the π-Electron Distribution. *Chem. Commun.* **2014**, *50*, 11118-11121.

[36] Anthony, J. E. The Larger Acenes: Versatile Organic Semiconductors, *Angew. Chem. Int. Ed.* **2008**, *47*, 452-483.

[37] Yang, Y.; Mosquera, M. A.; Skinner, K.; Becerra, A. E.; Shamamian, V.; Schatz, G. C.; Ratner, M. A.; Marks, T. J. Electronic Structure and Potential Reactivity of Silaaromatic Molecules, *J. Phys. Chem. A* **2016**, *120*, 9476-9488.

[38] Miao, Q. Ten Years of N-Heteropentacenes as Semiconductors for Organic Thin-Film Transistors, *Adv. Mater.* **2014**, *26*, 5541-5549.

[39] Baumgartner, T. Insights on the Design and Electron-Acceptor Properties of Conjugated Organophosphorus Materials, *Acc. Chem. Res.* **2014**, *47*, 1613-1622.

[40] Jutzi, P.; Deuchert, K. 9-Arsaanthracene, *Angew. Chem. Int. Ed.* **1969**, *8*, 991-992.

[41] Parker, T. M.; Burns, L. A.; Parrish, R. M.; Ryno, A. G.; Sherrill, C. D. Levels of Symmetry Adapted Perturbation Theory (SAPT). I. Efficiency and Performance for Interaction Energies. *J. Chem. Phys.* **2014**, *140*, 094106.

[42] Jeziorski, B.; Moszynski, R.; Szalewicz, K. Perturbation Theory Approach to Intermolecular Potential Energy Surfaces of van der Waals Complexes, *Chem. Rev.* **1994**, *94*, 1887-1930.

[43] Steinmann, S. N.; Corminboeuf, C. Comprehensive Benchmarking of a Density-Dependent Dispersion Correction. *J. Chem. Theory Comput.* **2011**, *7*, 3567-3577.

[44] te Velde, G.; Bickelhaupt, F. M.; Baerends, E. J.; Guerra, C. F.; Van Gisbergen, S. J. A.; Snijders, J. G.; Ziegler, T. Chemistry with ADF. *J. Comput. Chem.* **2001**, *22*, 931-967.

[45] Guerra, C. F.; Snijders, J. G.; te Velde, G.; Baerends, E. J. Towards an Order-N DFT Method. *Theor. Chem. Acc.* **1998**, *99*, 391-403.

[46] **ADF2016**, SCM, Theoretical Chemistry, Vrije Universiteit, Amsterdam, The Netherlands, http://www.scm.com.

[47] Rahm, M.; Hoffmann, R.; Ashcroft, N. W. Atomic and Ionic Radii of Elements 1–96. *Chem. Eur. J.* **2016**, *22*, 14625-14632.

[48] Batsanov, S. S. Van der Waals Radii of Elements. *Inorganic Materials* **2001**, *37*, 871-885.

[49] Kubas, A.; Hoffmann, F.; Heck, A.; Oberhofer, H.; Elstner, M.; Blumberger, J. Electronic Couplings for Molecular Charge Transfer: Benchmarking CDFT, FODFT, and FODFTB against High-Level Ab Initio Calculations. *J. Chem. Phys.* **2014**, *140*, 104105.

[50] Ringer, A. L.; Sherrill, C. D. First Principles Computation of Lattice Energies of Organic Solids: The Benzene Crystal. *Chem. Eur. J.* **2008**, *14*, 2542-2547.

[51] Wen, S.; Beran, G. J. O. Accurate Molecular Crystal Lattice Energies from a Fragment QM/MM Approach with On-the-Fly Ab Initio Force Field Parametrization. *J. Chem. Theory Comput.* **2011**, *7*, 3733-3742.

[52] Brandenburg, J. G; Grimme, S. Dispersion Corrected Hartree–Fock and Density Functional Theory for Organic Crystal Structure Prediction. *Top. Curr. Chem.* **2014**, *345*, 1-24.

[53] Vehoff, T.; Baumeier, B.; Troisi, A.; Andrienko, D. Charge Transport in Organic Crystals: Role of Disorder and Topological Connectivity. *J. Am. Chem. Soc.* **2010**, *132*, 11703-11708.